Inorganic Chemistry

Article

pubs.acs.org/IC

Mössbauer Spectroscopy as a Probe of Magnetization Dynamics in the Linear Iron(I) and Iron(II) Complexes $[Fe(C(SiMe_3)_3)_2]^{1-/0}$

Joseph M. Zadrozny,* Dianne J. Xiao, and Jeffrey R. Long*

Department of Chemistry, University of California, Berkeley, California 94720-1460, United States

Mihail Atanasov*,[†,‡] and Frank Neese*,[†]

[†]Max-Planck Institut fur Chemische Energiekonversion, Mulheim an der Ruhr, D-45470, Germany

[‡]Institute of General and Inorganic Chemistry, Bulgarian Academy of Sciences, Acad. Georgi Bontchev Str 11, 1113 Sofia, Bulgaria

Fernande Grandjean* and Gary J. Long*

Department of Chemistry, Missouri University of Science and Technology, University of Missouri, Rolla, Missouri 65409-0010, United States

Supporting Information

ABSTRACT: The iron-57 Mössbauer spectra of the linear, two-coordinate complexes, $[K(crypt\text{-}222)][Fe(C(SiMe_3)_3)_2]$, **1**, and $Fe(C(SiMe_3)_3)_2$, **2**, were measured between 5 and 295 K under zero applied direct current (dc) field. These spectra were analyzed with a relaxation profile that models the relaxation of the hyperfine field associated with the inversion of the iron cation spin. Because of the lifetime of the measurement (10^{-8} to 10^{-9} s), iron-57 Mössbauer spectroscopy yielded the magnetization dynamics of **1** and **2** on a significantly faster time scale than was previously possible with alternating current (ac) magnetometry. From the modeling of the Mössbauer spectral profiles, Arrhenius plots between 5 and 295 K were obtained for both **1** and **2**. The high-temperature regimes revealed Orbach relaxation processes with U_{eff} = 246(3) and 178(9) cm^{-1} for **1** and **2**, respectively, effective relaxation barriers which are in agreement with magnetic measurements and supporting ab initio calculations. In **1**, two distinct high-temperature regimes of magnetic relaxation are observed with mechanisms that correspond to two distinct single-excitation Orbach processes within the ground-state spin−orbit coupled manifold of the iron(I) ion. For **2**, Mössbauer spectroscopy yields the temperature dependence of the magnetic relaxation in zero applied dc field, a relaxation that could not be observed with zero-field ac magnetometry. The ab initio calculated Mössbauer hyperfine parameters of both **1** and **2** are in excellent agreement with the observed hyperfine parameters.

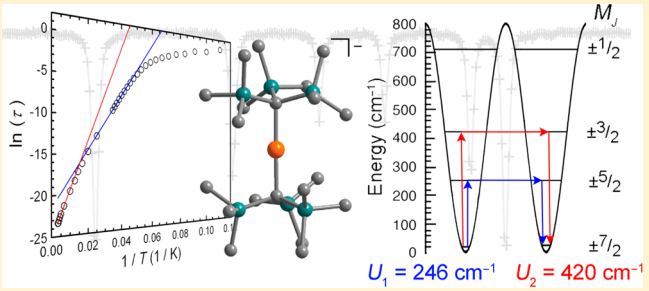

INTRODUCTION

The study of magnetic relaxation in mononuclear complexes of lanthanide and transition metal ions, first pursued in depth nearly 75 years ago,[1] has been of renewed interest because of the discovery of their utility as single-molecule magnets[2] in 2003 and 2010, respectively.[3,4] In these compounds, because of their axially bistable magnetic moments, the constituent paramagnetic metal ions may be magnetized and retain their magnetization as a consequence of a potential energy barrier to spin reversal, U. Further discoveries of large barriers for such lanthanide[5] and transition metal[6] single-molecule magnets relative to their multinuclear counterparts have inspired a widespread research effort aimed at preparing mononuclear complexes with ever-higher relaxation barriers. Note that complexes possessing such axially bistable magnetic moments may one day find potential application as media for high-density information storage,[7] but moreover they have served as a fertile platform for the study and elucidation of the low-temperature physics of inherently quantum entities, ultimately leading to the suggestion that single-molecule magnets can behave as qubits.[8]

Paramount to the development of single-molecule magnets as a useful technology is an exact knowledge of which factors engender a large relaxation barrier. While the origins of some of the factors that contribute to U are known, in practice there are a variety of effects that can lessen the effective (or measured) magnitude of U, U_{eff}. Thus, the a priori design of molecules

Received: August 5, 2013
Published: October 31, 2013

   dx.doi.org/10.1021/ic402013n | Inorg. Chem. 2013, 52, 13123−13131

with large effective barriers has not proven completely straightforward. In particular, computational efforts[9] have revealed U_{eff} to be very sensitive to small distortions of the coordination environment of the spin-bearing metal cations. Thus, predictions based upon symmetry-idealized model geometries may not hold for crystalline structures, because small structural distortions away from idealized symmetries can easily arise from sources such as crystal packing, which are difficult to model. Rather recently, vibronic coupling has also been implicated as an influence for the spin-reversal barrier height, although this phenomenon can not as yet be fully treated from a computational perspective.[10] Unambiguous determination of the observed relaxation barriers for mononuclear single-molecule magnets is thus necessary for developing an in depth understanding of the factors that control the barrier heights in such systems.

The determination of the intrinsic relaxation barrier height possessed by a molecule is typically performed by an analysis of the temperature dependence of the magnetic relaxation time, τ, with alternating current (ac) magnetic susceptibility studies and a subsequent construction of an Arrhenius plot.[2] When spin or magnetization reversal occurs via an Orbach process,[11] τ displays an exponential relationship with temperature such that the analysis produces a straight line in the Arrhenius plot with a slope equal to U_{eff}/k_B, where k_B is the Boltzmann constant. Note that other non-Orbach relaxation processes, such as quantum tunneling of the magnetization,[12] Raman,[11,13] and direct[14] relaxation, are also commonly operative and do not display an exponential temperature dependence of their associated relaxation times. Thus, if these relaxation processes are significant in the magnetization dynamics of a complex, the Arrhenius plot will depart from linearity and can display substantial curvature or even near temperature-independence of τ. The assignment of Orbach relaxation by inspection of such curved Arrhenius plots can be fraught with difficulty. One common attempt at overcoming this problem involves the judicious exclusion of low-temperature relaxation data and Arrhenius analysis of a small set of the high-temperature τ values to approximate U_{eff}. An alternate procedure models the temperature dependence of τ as a sum of contributions from the various mentioned relaxation processes. However, in both cases it should be noted that substantial curvature in Arrhenius plots often persists even to high temperatures in some complexes and thus a substantial level of uncertainty is imparted in the derived U_{eff} values.

Of utility, therefore, are techniques that allow for the determination of the relaxation time at high temperatures, since such techniques would give unique and valuable information when the magnetic relaxation times are shorter than those measurable with the ac drive of a commercial SQUID magnetometer. Mössbauer spectroscopy has recently been shown to satisfy this requirement via the application of a formalism, developed in 1974 by Dattagupta and Blume,[15] that was used to model the paramagnetic relaxation broadening of the spectra of three-[16] and four-coordinate[4] iron(II) complexes and determine the activation energy for relaxation from Arrhenius plots.

This year, we described the low temperature magnetization dynamics of two linear species containing iron(I) and iron(II) ions coordinated by the tris(trimethylsilyl)methido ligand, $[K(crypt\text{-}222)][Fe(C(SiMe_3)_3)_2]$, **1**, and $Fe(C(SiMe_3)_3)_2$, **2**. These complexes exhibit very large spin reversal barriers of 226 and 146 cm^{-1}, under zero and modest applied direct current (dc) fields, respectively,[6h,j] as a result of nearly unquenched orbital angular momentum.[17] For both **1** and **2**, however, the Arrhenius plots are substantially curved, and thus the U_{eff} values were obtained, respectively, by using both of the above-mentioned approaches for overcoming the problem of curved Arrhenius plots. Herein, we report the application of Mössbauer spectroscopy to evaluate the magnetization dynamics of **1** and **2** from 5 to 295 K. The technique helped elucidate the mechanism of slow magnetic relaxation in these complexes and furthermore provided Mössbauer spectral parameters which are compared with the results of ab initio computations.

EXPERIMENTAL SECTION

Sample Preparation and Instrumentation. Fresh samples of **1** and **2** were synthesized according to the published procedures[6j,18] and, respectively, either recrystallized or sublimed prior to study. The iron-57 Mössbauer spectra of **1** and **2** were obtained between 5 to 295 K with a constant acceleration spectrometer and a cobalt-57 rhodium source. Prior to measurements the spectrometer was calibrated at 295 K with α-iron foil. Powder absorbers of thicknesses of 100 and 50 mg/cm^2, or 6.0 and 5.4 mg of iron per cm^2, respectively, were prepared and transferred to the coldfinger of a closed-cycle refrigerator under an inert atmosphere to avoid oxidation of these highly air-sensitive compounds.

Ab Initio Computational Methods. Mössbauer spectral parameters have been computed with the ORCA program.[19] The Mössbauer spectral isomer shifts, δ, were calculated using density functional theory (DFT) and the experimental X-ray diffraction structures of **1** and **2** and the GGA(BP86) functional[20] with the standard triple-ζ basis set of Ahlrichs and co-workers.[21] The DFT calibration for the isomer shift in mm/s relative to α-iron at 295 K (eq 1) was performed using experimental data for a test set of molecules, as was previously described.[22]

$$\delta = -0.340(\rho(0) - 11580) + 1.034 \quad (1)$$

Charge densities at the iron nuclei, $\rho(0)$, for **1** and **2** from these calculations are 11582.110069 and 11581.571691 a_0^{-3}, respectively, which after substitution yield δ values of 0.316 and 0.500 mm/s. These values agree well with results reported previously and herein.[6j,17]

In contrast, the same DFT calculations yielded quadrupole splittings, $e^2Qq/2$, of −1.653 mm/s for **1** and −1.399 mm/s for **2**, values that, especially for **1**, are in less satisfactory agreement both with the results reported below and with previous results. The less than satisfactory agreement between the density functional calculated and experimental quadrupole splitting for **1** results from the single reference ground state assumed in this calculation, an assumption that is not valid for **1** and is poor for **2**, in which the electronic ground state is formed by a mixture of different electronic configurations. Hence, multireference CASSCF and NEVPT2 calculations were carried out. Nuclear quadrupole mixing between the degenerate electronic sublevels of the respective ^4E and ^5E ground states of **1** and **2** renders the calculation of $e^2Qq/2$ by first principles theoretically challenging. Note that the 10^{-4} cm^{-1} magnitude of the quadrupole interaction is significantly smaller than the expected energies of the geometric distortions and spin−orbit coupling. Thus, we can safely assume that state-specific values of $e^2Qq/2$ are reasonably well-defined, and it is under this assumption that the multireference calculations of the quadrupole splitting and asymmetry parameter, η, were performed herein.

The general procedure used for these calculations is as follows: (1) The electric field gradient tensors for **1** and **2** were computed on the basis of orbital gradients from converged CASSCF wave functions. (2) The converged CASSCF/NEVPT2 calculations were then repeated to yield nonrelativistic eigenvalues and eigenvectors for each non-relativistic electronic state. In these calculations, all 10 quartet and 5 quintet states for **1** and **2**, respectively, were used. (3) The resultant spin−orbit coupled eigenfunctions and the field gradient tensors in the

dx.doi.org/10.1021/ic402013n | Inorg. Chem. 2013, 52, 13123−13131

nonrelativistic basis of configuration state functions, corresponding to eigenfunctions of the $\hat{S}^2$ and $\hat{S}_z$ operators, were transformed to electric field gradient tensors for each spin eigenstate of the nonrelativistic Born−Oppenheimer Hamiltonian. (4) The nonrelativistic electric field gradient tensors were then transformed to the relativistic ones using the eigenvectors of the spin−orbit coupling operator (eq 2),

$$V_{ij}(\mu) = \sum_k c(k, \mu)^* c(k, \mu) V_{ij}(k) \quad (2)$$

where k and μ enumerate nonrelativistic and relativistic eigenstates, respectively. These tensors were then diagonalized to yield the values of $e^2Qq/2$ and η.

The calculation of $e^2Qq/2$ and η for **2** required a slight modification of the above procedure. In particular, mixing between the $d_{x^2-y^2}$ and d_{xy} components of the ^5E ground state, which is split because of a small orthorhombic distortion, leads to a large calculated η value for the complex, a value that is unexpected given the high molecular symmetry of **2**. State specific nonrelativistic field gradient tensors were therefore computed for the D_{3h}-symmetric model complex $Fe(CH_3)_2$. When utilized in the calculations with the spin−orbit eigenvectors of **2** computed from its X-ray diffraction structure, these tensors lead to $e^2Qq/2$ and η values in excellent agreement with experimental values. Specific values obtained for the two lowest spin−orbit coupled states of **1** and **2** are given in Table 1.

Table 1. Calculated $e^2Qq/2$ and η for the Lowest-Lying M_J Doublet States

	M_J	energy,[a] cm^{-1}	$e^2Qq/2$, mm/s	η
$[Fe(C(SiMe_3)_3)_2]^-$, **1**	±5/2	210	−2.640	0.005
	±7/2	0	−2.611	0.004
$Fe(C(SiMe_3)_3)_2$, **2**	±3	195.2, 195.3	−1.161	0.003
	±4	0, 0.001	−1.145	0.001

[a]The relative ab initio energies of the low-lying M_J states.

RESULTS AND DISCUSSION

Temperature Dependence of the Mössbauer Spectra.

The iron-57 Mössbauer spectra of **1** and **2** obtained at various temperatures between 5 and 295 K are shown in Figures 1 and 2, respectively. At low temperature, both complexes display sharp sextets; the sextet of **1** spans ±12 mm/s whereas that of **2** has a much larger splitting and spans ±25 mm/s. With increasing temperature, these sextets remain relatively sharp and unchanged until a certain temperature, above which they broaden considerably. In **1**, the sextet persists up to 30 K, then broadens slightly at 40 K, and then more extensively between 50 and 70 K. In contrast, the spectrum of **2** remains relatively unchanged up to 25 K, whereupon it begins to broaden. At 80 and 100 K, a sharp central absorption line is observed for **1**, and at temperatures above 150 K, the spectrum is resolved into an asymmetric doublet. For **2**, a central absorption line is also observed at 106 K, but unlike **1**, this absorption remains mostly unresolved even at 295 K.

The observed temperature dependence of the Mössbauer spectral line shape profiles of **1** and **2** is characteristic of relaxation of the hyperfine field on a time scale that is comparable with the Larmor precession time of the iron-57 nuclear moment about the hyperfine field, corresponding to 10^{-8} to 10^{-9} s depending upon the magnitude of the hyperfine field, see the Supporting Information for more details.[23−25] In **1**, at 5 K, the iron-57 nucleus experiences an effectively static hyperfine field, and the line width observed at 5 K is the experimental line width of 0.295(5) mm/s; this line width agrees well with that of α-iron foil obtained at 5 K and ±25 mm/s under virtually the same experimental conditions. Note that this particular observation is in accord with the previously collected ac susceptibility results obtained in zero dc field, results which revealed relaxation times of about 1.5 s or more

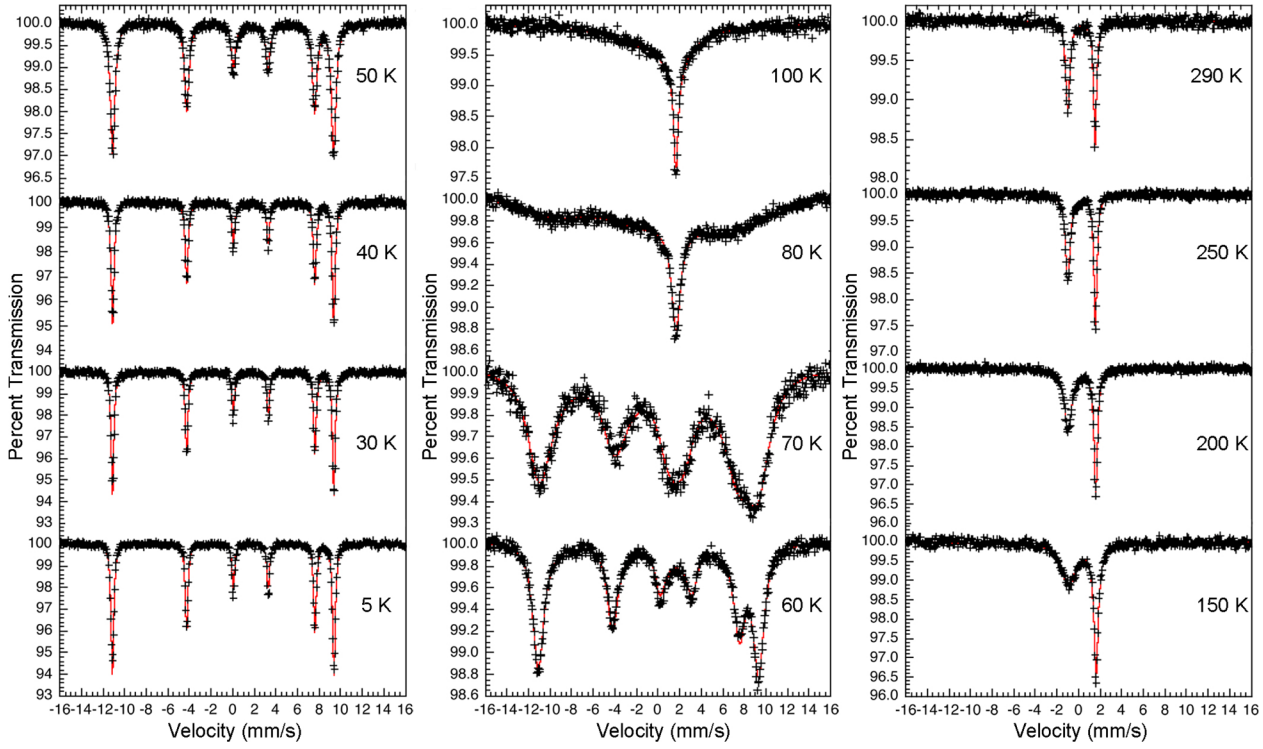

Figure 1. Iron-57 Mössbauer spectra of **1** obtained at the indicated temperatures. Solid red lines are fits with a relaxation profile, as discussed in the text.

dx.doi.org/10.1021/ic402013n | Inorg. Chem. 2013, 52, 13123−13131

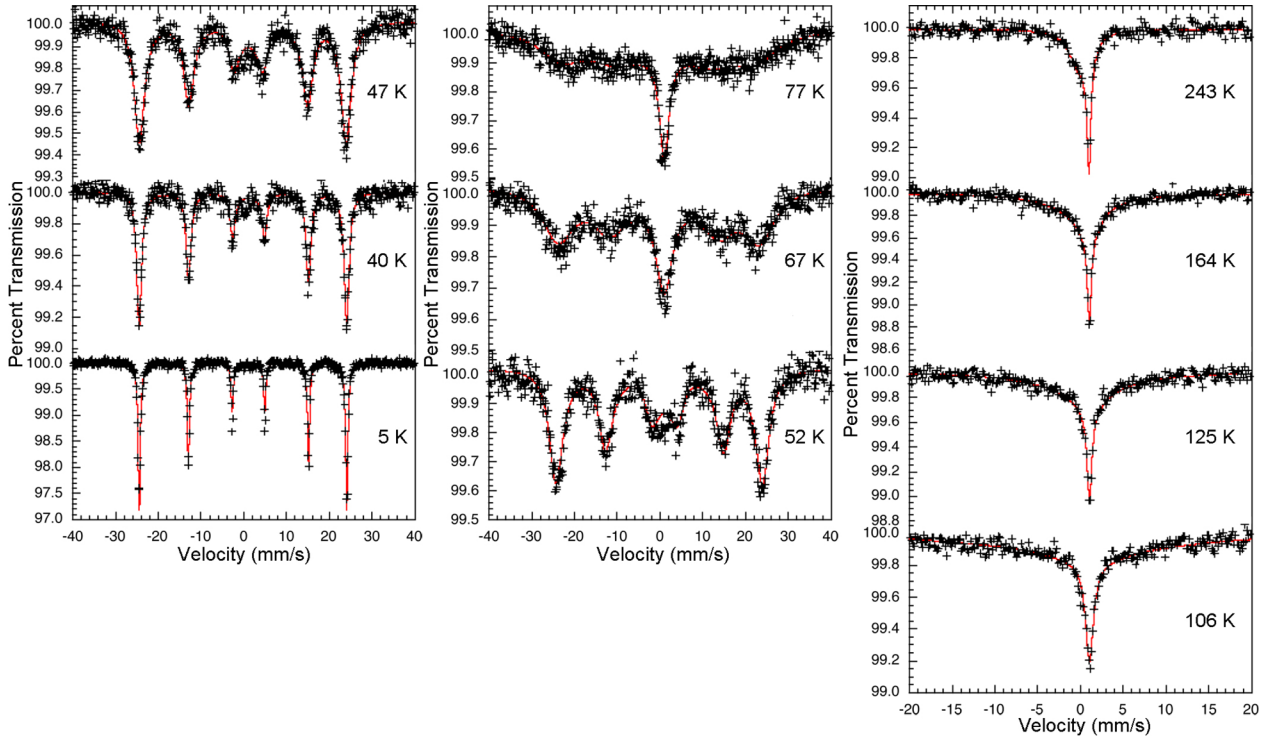

Figure 2. Iron-57 Mössbauer spectra of **2** obtained at the indicated temperatures. Solid red lines are fits to a relaxation profile, as discussed in the text.

below 9 K, corresponding to a time scale that is much longer than the Larmor precession time of the iron-57 nuclear moment about the hyperfine field. In contrast to the spectra of **1**, the spectrum of **2**, which appears to be very sharp at 5 K, actually has a line width of 0.650 mm/s, a line width that is twice the calibration line width of 0.326(5) mm/s observed at ±40 mm/s for α-iron at 5 K.

Extraction of the effective internal hyperfine field, H_{int}, isomer shift, δ, and quadrupole splitting, $e^2Qq/2$, in the presence of the strong influence of slow magnetic relaxation requires modeling the relaxation profile. Thus, the spectra for both **1** and **2** were fitted with a relaxation model of the hyperfine field by using the Dattagupta and Blume[15] formalism. In this fitting model, the hyperfine field was assumed to be oriented parallel to the principal axis of the electric field gradient tensor, taken as the C−Fe−C linear axis with η, the asymmetry parameter of the electric field gradient tensor, fixed at zero. This hyperfine field reverses along this axis with a relaxation frequency, ν, or with a relaxation period, $\tau = 1/\nu$. Because the relaxation of the hyperfine field leads to a broadening of the spectral lines, as is observed in the spectra of **1** above 40 K and **2** between 5 and 295 K, a minimum experimental line width, as well as a constant hyperfine field, were determined as follows and used to fit the spectra to obtain a reliable temperature dependence of the relaxation period for both **1** and **2**.

For complex **1**, fits below 40 K indicate no broadening of the lines through relaxation. Further, the hyperfine field decreases only very slightly from 63.68(2) T at 5 K to 63.61(2) T at 30 K. Hence, in the relaxation fits performed above 40 K for **1**, the value of H_{int} was constrained to 63.55 T, a value obtained from fitting the 40 K spectrum in the absence of relaxation. The higher-temperature spectra were also fitted with the relaxation model described above for a fixed line width of 0.295 mm/s; the resulting spectral parameters are reported in Table 2 and Supporting Information, Table S1, and the fitted profiles are shown as the red lines in Figure 1.

Table 2. Selected Experimental and Calculated Mössbauer Spectral Parameters

	T, K	**1**	**2**
δ, mm/s[a]	295	0.270(4)	0.292(7)
δ, mm/s[a]	5	0.402(1)	0.460(3)
δ_{calc}, mm/s[a]		0.316	0.500
$e^2Qq/2$, mm/s	295	−2.523(7)	−1.275
$e^2Qq/2$, mm/s	5	−2.555(2)	−1.275(5)
$e^2Qq/2_{calc}$, mm/s		−2.611	−1.145
H_{int}, T	5	63.68(2)	150.7(1)
H_{int}, T[b]		63.55	150.7
Γ_{exp}, mm/s[b]		0.295	0.326
Θ_M, K		313(16)	180(10)
Θ_D, K		141(2)	125(7)
η_{exp}		0	0
η_{calc}		0.004	0.001

[a]The isomer shifts are given relative to α-iron foil at 295 K. [b]The values of the parameters used in the relaxation fits.

For compound **2**, the spectra were fitted using a similar model, in which the experimental line width, hyperfine field, and quadrupole splitting were constrained to 0.326 mm/s, 150.7 T, and −1.275 mm/s, respectively. The fits obtained are shown as the red lines in Figure 2 and the resulting parameters are given in Tables 2 and Supporting Information, Table S2.

The temperature dependences of the isomer shift and logarithm of the spectral absorption areas of **1** and **2** are shown in Figures 3 and 4, where the solid lines are the result of fits[26] with the Debye model for a solid. In contrast to these two

dx.doi.org/10.1021/ic402013n | Inorg. Chem. 2013, 52, 13123−13131

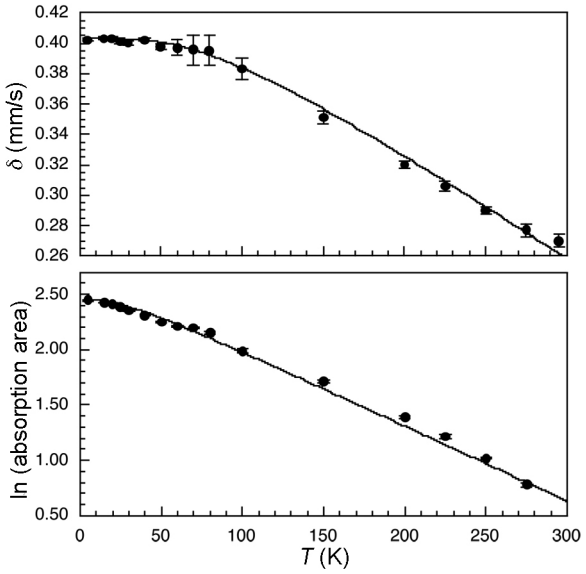

Figure 3. Temperature dependence of the isomer shift, top, and spectral absorption area, bottom, of **1**. The solid lines are the results of fits with the Debye model for a solid. The error bars are shown but are often as small as the data points.

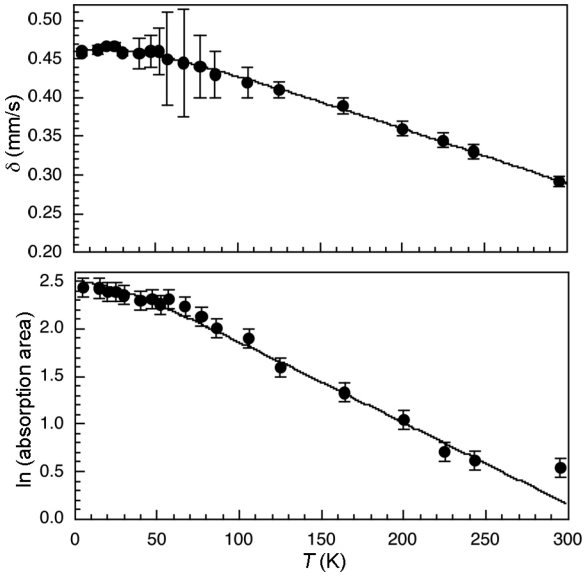

Figure 4. Temperature dependence of the isomer shift, top, and spectral absorption area, bottom, of **2**. The solid lines are the results of fits with the Debye model for a solid. The error bars are shown but are sometimes as small as the data points.

parameters, which are temperature-dependent, the values of $e^2Qq/2$ for **1** and **2** at 5 K, −2.555(5) and −1.275(5) mm/s, respectively, are relatively independent of temperature. Note that the calculated $e^2Qq/2$ values for the two lowest-lying states for **1** and **2** (see Table 1) are nearly the same, suggesting that with increasing temperature, population of the excited M_J doublets is not expected to yield appreciable temperature dependence of the quadrupole splitting. The Mössbauer temperature, Θ_M, and the Debye temperature, Θ_D, for **1**, obtained from a fit of the temperature dependence of the isomer shift and spectral absorption area are 313(16) and 141(2) K, respectively. In contrast, Θ_M and Θ_D for **2** are 180(10) and 125(1) K, respectively, as determined in the same manner. Here, the larger temperatures obtained for **1** as compared to **2** likely result from the somewhat larger lattice energy of the ionic lattice of **1** as compared with the presumably lower lattice energy of the molecular complex **2**. Furthermore, Debye temperatures of about 150 K are characteristic[27,28] of organometallic compounds, and it is well-known that Θ_M is typically observed to be 2 to 3 times larger than Θ_D because the temperature dependence of the isomer shift is more sensitive to the higher energy phonons than the temperature dependence of the spectral absorption area.

The H_{int} values of 63.55 and 150.7 T used for the calculation of the relaxation profiles for **1** and **2**, respectively, are the vector sums of three contributions, the Fermi contact field, H_{Fermi}, the dipolar field, H_{dip}, and the orbital field, H_{orb}. A possible fourth contribution originating from magnetic moments on other iron cation sites in the lattice may be neglected[29] because the iron cation containing clusters are well-isolated from each other. The H_{Fermi} value is known to be negative and may be estimated from $-2S(12.7)$ T to be −38 T for $S = {}^3/_2$ in **1** and −51 T for $S = 2$ in **2**. The H_{dip} value is approximately proportional to the quadrupole splitting and is estimated to be +24 and +12 T in **1** and **2**, respectively. Because the H_{orb} is opposite in sign to H_{Fermi}, the observed effective hyperfine fields can only be positive and yield large positive orbital contributions of about +78 and +191 T in **1** and **2**, respectively.

The isomer shifts in **1** and **2** are lower than might be expected for iron(I) and iron(II). However, the low values are consistent with two-coordinate complexes; it is well-known[30] that the iron(II) isomer shift decreases with decreasing coordination number. Further, it should be noted that the decrease in isomer shift from **2** to **1** might be unexpected on the basis of a change from a $3d^6$ to a $3d^7$ electronic configuration. However, the very strong 4s-$3d_{z^2}$ mixing predicted in **1** by ab initio calculations[6j] should yield an increased 4s electron density at the iron-57 nucleus and thus decrease the observed isomer shift. A similar influence of strong 4s-$3d_{z^2}$ mixing on the isomer shift of iron(I) in $Li_2[(Li_{0.79}Fe_{0.21})N]$ was reported in 2002.[31] In this latter compound, the iron(I) is in an infinite chain $^1{}_\infty[(Li_{1-x}Fe_x)N]$ and is linearly coordinated to two nitrogen atoms along the chain and to lithium(I) and iron(I) in the plane perpendicular to the chain. Its isomer shift of between 0.17 mm/s at 4.2 K and −0.026 mm/s at 295 K is even smaller than is observed for **1**. Additional similarity to **1** is found in the approximately temperature-independent quadrupole interactions of −2.56 to −2.61 mm/s[31] observed in $Li_2[(Li_{1-x}Fe_x)N]$. Further, the obtained values of H_{orb} and H_{Fermi} obtained for **1** compare well with those observed and calculated[29,31] with a variety of computational methods in $Li_2[(Li_{1-x}Fe_x)N]$.

Calculated and Observed Mössbauer Spectral Parameters. The calculated and observed isomer shifts in **1** and **2** are in good agreement as indicated in Table 2. Further, the decrease in isomer shift from **2** to **1** is well reproduced by the calculations and results, as indicated above, from the strong 4s-$3d_{z^2}$ mixing. Of particular note are the rather large, negative values of the observed quadrupole splittings in **1** and **2**. It is customary in the study of Mössbauer spectra to analyze the quadrupole splitting in terms of a lattice and a valence contribution. In octahedral iron(II) complexes, the theoretical approach developed by Ingalls[32] has found wide acceptance. It is somewhat surprising that this classical crystal field approach fails in the case of **1** and **2**, as is discussed in more detail in the

dx.doi.org/10.1021/ic402013n | Inorg. Chem. 2013, 52, 13123−13131

Supporting Information. Herein, however, the very negative quadrupole splittings of **1** and **2** and the expected zero asymmetry parameter could only be reproduced by multi-reference calculations for each electronic state of the ^{4}E and ^{5}E ground states of **1** and **2**. These more comprehensive calculations gave an essentially zero asymmetry parameter and quadrupole splitting values for **1** and **2** that agree within 0.1 mm/s with the 5 K observed values, as is shown in Table 2.

Dynamics of the Hyperfine Field and Spin Reversal. The fits of the Mössbauer spectra of **1** and **2** provided the hyperfine field relaxation frequencies at temperatures up to 295 K, frequencies that can be as fast as 15000 MHz. These results were used to derive magnetic relaxation times and subsequently construct Arrhenius plots for **1** and **2**, as shown in Figure 5. Note that, although relaxation times for **2** could be derived down to 5 K, the relaxation times for **1** below 40 K could not be obtained because the time scale of the relaxation at these temperatures is much longer than the Larmor precession time. At 40 K the relaxation time for **1** is 290(30) × 10^{-8} s, and it rapidly decreases with increasing temperature, ultimately reaching 0.0071(6) × 10^{-8} s at 295 K. In contrast, from 5 to 25 K, the relaxation time for **2** remains relatively constant at 25(1) × 10^{-8} s. However, at and above 30 K, τ decreases considerably, reaching 0.0119(8) × 10^{-8} s at 295 K.

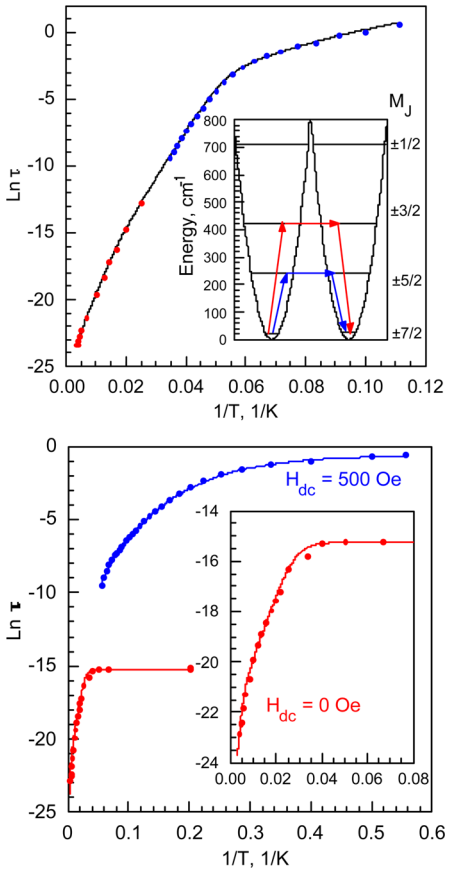

Figure 5. Arrhenius plots for **1** and **2** as obtained from Mössbauer spectroscopy and ac susceptibility, where τ is in units of seconds. Top: relaxation time for **1** obtained from Mössbauer spectra, red, and from ac-susceptibility results, blue, reported in ref 6j. The black line is the result of the fit described in the text. Inset: energies of the M_J = ±7/2, 5/2, and 3/2 doublets as determined by a combined ac susceptibility and Mössbauer spectral study and the M_J = ±1/2 doublet at an energy determined theoretically in reference 6j; the blue and red arrows indicate the two observed Orbach relaxation pathways. Bottom: relaxation time for **2** obtained from Mössbauer spectra, red, and from ac-susceptibility results,[6h] blue. The red and blue lines are the result of fits described in the text. Inset: expanded view of the Arrhenius plot above 5 K.

The temperature dependence of the relaxation time yields vital information about the pathways for magnetic relaxation in **1** and **2**. A detailed analysis of the Arrhenius plots was therefore carried out; for **1** this plot includes relaxation times obtained from both Mössbauer spectroscopy and ac magnetic susceptibility measurements.[6h,j] In particular, we modeled the relaxation times from 5 to 295 K for both **1** and **2** as respective sums of tunneling, Raman, and Orbach processes (eq 3),

$$\tau^{-1} = \tau_{QTM}^{-1} + CT^5 + \tau_{0,1}^{-1}\exp(-U_1/k_BT) + \tau_{0,2}^{-1}\exp(-U_2/k_BT) \quad (3)$$

where τ_{QTM} corresponds to the relaxation time of the tunneling relaxation process and C is the Raman coefficient. The last two terms of eq 3 correspond to two separate Orbach processes, where $\tau_{0,1}^{-1}$ and $\tau_{0,2}^{-1}$ are the respective attempt frequencies, and U_1 and U_2, are the respective effective magnetization reversal barriers. The zero applied dc field conditions, under which the Mössbauer spectra of **1** and **2** were measured, eliminated the necessity of a direct relaxation term AH^2T in the above equation. Previous relaxation time results were collected for **1** at zero applied dc field by ac-susceptibility measurements in the frequency range of 0.1 to 1500 Hz, and these results were combined with Mössbauer spectral relaxation times to provide a comprehensive picture of the temperature dependence of the magnetization dynamics for **1** and **2**.

The τ^{-1} values obtained for **1** above 9 K, that is, at temperatures above the tunneling regime, were fitted without the inclusion of τ_{QTM}^{-1}. In contrast, for **2** the τ_{QTM}^{-1} term was required to obtain a good fit. Further, the data for **1** and **2** could only be well fitted at the highest temperatures if two Orbach processes were included. The best fit for **1** above 9 K yields C = 8.1(2) × 10^{-7} s^{-1} K^{-5}, $\tau_{0,1}^{-1}$ = 2.2(4) × 10^9 s^{-1}, U_1 = 246(3) cm^{-1}, $\tau_{0,2}^{-1}$ = 1.03(7) × 10^{11} s^{-1}, and U_2 = 420(9) cm^{-1}. The best fit for **2** between 5 and 295 K yields τ_{QTM}^{-1} = 4.2(3) × 10^6 s^{-1}, C = 4.3(7) × 10^{-4} s^{-1} K^{-5}, $\tau_{0,1}^{-1}$ = 5(1) × 10^9 s^{-1}, U_1 = 178(9) cm^{-1}, $\tau_{0,2}^{-1}$ = 1(2) × 10^{11} s^{-1}, U_2 = 553(68) cm^{-1}. The individual contributions of each relaxation process to the full Arrhenius plots of **1** and **2** are depicted in Supporting Information, Figures S1 and S2.

The significance of these results is readily evaluated in comparison with those obtained from previous measurements. For **1**, note that the value of U_1 does not change upon inclusion of the other relaxation processes, whereas for **2**, U_1 is nearly 30 cm^{-1} larger than that obtained via ac susceptibility. It is of interest here that the present U_1 = 178(9) cm^{-1} for **2** is much closer to the ab initio value of 196 cm^{-1}, which is consistent with a more accurate Arrhenius analysis conducted here in the absence of the direct process. Note that in **2**, the temperature independent regime below 25 K, with a relaxation time of 0.25 μs, highlights why zero-field ac susceptibility studies were impossible for **2** in the accessible frequency range. However, the two data sets together demonstrate the remarkable power of the applied dc field, which slows the magnetic relaxation time for **2** by approximately 7 orders of magnitude over only a 500 Oe difference in field strength.

The necessity of an applied field to observe slow magnetic relaxation by ac susceptibility in **2** versus **1** is likely tied to the

dx.doi.org/10.1021/ic402013n | Inorg. Chem. 2013, 52, 13123−13131

spin parity of the two species, where **1** is a half integer spin system versus **2**, which is integer spin. Thus far, only half-integer spin complexes in a zero applied dc field have exhibited magnetic relaxation times long enough for ac susceptibility analysis.[6e,g,j,k] Previous studies on integer-spin complexes have linked the requirement of the applied field to nonzero transverse anisotropies,[4b,6h] anisotropies which can result from slight deviations of the molecular symmetry from idealized axially symmetric environments and result in fast quantum tunneling pathways for magnetic relaxation.[12] For **1** and **2**, we note that the coordination geometries for both species are linear, where **2** possesses molecular D_{3d} symmetry with perfectly staggered $[C(SiMe_3)]^-$ ligands and equivalent Fe−C distances of 2.051(1) Å. In contrast, the Fe−C distances in the two nearly eclipsed $-SiMe_3$ moieties of the $[C(SiMe_3)_3]^-$ ligands in **1** are not crystallographically constrained to be equivalent, and the observed very similar Fe−C distances of 2.058(4) and 2.063(4) Å lead to a relatively lower overall symmetry. Thus, one might expect the fast magnetic relaxation via tunneling to be more prevalent in **1** than **2**, but this is not the case. This observation of slower magnetic relaxation times for **1** compared to **2** at zero applied dc field likely reflect the relatively lesser ability of transverse anisotropy to engender fast magnetic relaxation in half-integer mononuclear species, and may be one of the major reasons why two relaxation barriers are clearly resolved for **1** but less clearly for **2**.

A reviewer of this paper has suggested that the slight mismatch in the intensity of the inner lines and the broad lines of the 5 K Mössbauer spectrum of **2**, see Figure 2, are indicative of a narrow hyperfine field distribution of about 1 T about the 150.7 T observed hyperfine field, rather than slow magnetic relaxation. However, the source of such a narrow distribution is very difficult to identify. A possible source could be the presence of dynamic vibronic coupling inducing a structural disorder, but the existence of such coupling is not supported by the temperature dependence of the dc-magnetic susceptibility, which is well described[10] with a static model. If this distribution is present between 5 and 25 K, then the resultant broadening hides or combines with any effect of quantum tunneling of the magnetization. If the broadening is entirely due to the hyperfine field distribution, then the quantum tunneling relaxation rate is smaller than 3.8 MHz, see Supporting Information, Table S2, and larger than the highest frequency of 1.5 kHz probed[6h] by ac-susceptibility. In view of an unidentifiable source of hyperfine field distribution and its entanglement with the effect of quantum tunneling of the magnetization, the assignment of the broadening observed between 5 and 25 K in the Mössbauer spectra of **2** to quantum tunneling of the magnetization is preferred as most likely. Further, the possible presence of the small field distribution does not affect the interpretation of the higher-temperature Mössbauer spectra as proposed here.

Of special interest is the observation of two regimes of thermally assisted magnetic relaxation in **1** and **2**. The above analysis of **1** revealed that the magnetic moment of the $J = {}^7/_2$ iron(I) center in **1** required 246 cm^{-1} for spin reversal, a finding which closely matched the calculated 199 cm^{-1}, obtained from the CASSCF computation, and the 210 cm^{-1}, obtained from the NEVPT2 computation, energy separations between the ground $M_J = \pm{}^7/_2$ and the first excited $M_J = \pm{}^5/_2$ levels. The remarkable agreement between the NEVPT2 value of 210 cm^{-1} and the experimental value of 246 cm^{-1} results probably from the inclusion of dynamical correlations in the NEVPT2 calculations. Our observations seem to coincide with those made in many mononuclear transition metal and lanthanide single-molecule magnets, for which derived magnetic relaxation barriers are found to correspond approximately to the determined energy separations between the ground M_S or M_J state and the first excited M_S or M_J state. Similar analyses of **2** revealed spacings between the ground $M_J = \pm4$ and $M_J = \pm3$ levels to be 196 cm^{-1}, which is close to the observed U_1 value for **2**. This seemingly general observation is in contrast to multinuclear single-molecule magnets. For example, the original single-molecule magnet, $Mn_{12}O_{12}(O_2CCH_3)_{16}(H_2O)_4$,[2,33] with a ground state spin of $S = 10$ and a zero-field splitting energy, D, of 0.5 cm^{-1}, exhibits a 9.5 cm^{-1} splitting between its $M_S = \pm10$ and lowest-lying $M_S = \pm9$ states, yet the observed barrier is 42 cm^{-1}, a value much larger than the first-excitation. Therefore, in $Mn_{12}O_{12}(O_2CCH_3)_{16}(H_2O)_4$ there must be successive excitations from $M_S = \pm10$ to $M_S = \pm9$ to $M_S = \pm8$ and so forth until an effective top of the spin reversal barrier is approached, where the spin is allowed to reverse. This situation is frequently encountered in other multinuclear single-molecule magnets.[2]

At temperatures above 50 K, **1** appears to relax via a thermally assisted process with a much larger barrier of $U_2 = 420$ cm^{-1}. Note that this value approaches the energy splitting between the $M_J = \pm{}^7/_2$ and $M_J = \pm{}^3/_2$ levels obtained from computation, which is 435 cm^{-1} by CASSCF and 452 cm^{-1} by NEVPT2 computations. A similar behavior is seen in **2** above 200 K; however, the agreement between $U_2 = 553(68)$ cm^{-1} and the computed gap between the ground, $M_J = \pm4$, and second excited doublets, $M_J = \pm2$, of 353 and 445 cm^{-1} for **2** is not as satisfactory as for **1**, most likely because of the relatively small amount of data used to obtain U_2. Hence, we will not discuss any further the relaxation process in **2**. At this point, it is difficult to diagnose whether the high-temperature regime is one in which magnetic relaxation proceeds via a single-excitation from the $M_J = \pm{}^7/_2$ doublet to the $M_J = \pm{}^3/_2$ doublet or from two successive excitations, $M_J = \pm{}^7/_2$ to $M_J = \pm{}^5/_2$ to $M_J = \pm{}^3/_2$. On the basis of the experimental data, the barrier observed in the regime of 9 to 50 K requires phonons of 246 cm^{-1}, and therefore a second excitation, to realize a total barrier of 420 cm^{-1} for **1**, would need an additional phonon of only 174 cm^{-1}, that is, less than that required for the initial excitation. Thus, it appears that, like the low-temperature Orbach process, the high-temperature Orbach process for **1** proceeds via a single excitation.

As for most, if not all, mononuclear single-molecule magnets, the question of why the magnetic relaxation occurs via a single excitation may be related to the mixing of the excited $\pm M_J$ doublets. Here, any significant amount of mixing in an excited state engenders tunneling to the other side of the relaxation barrier. Therefore, such mixing may give rise to U_{eff} barriers matching the energy of that specific excited state relative to the ground state. In contrast, a relatively low amount of mixing may instead force the system to relax via proceeding to higher excited levels, which may be more strongly mixed. Note that in general such mixing is likely to increase as the value of $|M_J|$ (or $|M_S|$ for systems with quenched orbital angular momentum) decreases. However, it should also be pointed out that $[Co(SPh)_4]^{2-}$ and $(PNP)FeCl_2$ (PNP^- = N[2-P($CHMe_2$)$_2$-4-methylphenyl]$_2$ anion),[6e,g] which are $S = {}^3/_2$ systems that show slow magnetic relaxation under a zero applied dc field, necessarily possess extremely weak mixing within the $M_S = \pm{}^3/_2$ Kramers doublet. In the context of **1**, then, it is not completely clear why the magnetic moment, at low temper-

dx.doi.org/10.1021/ic402013n | Inorg. Chem. 2013, 52, 13123−13131

ature, is exclusively excited to $M_J = \pm^5/_2$ prior to reversal as opposed to proceeding up to the $M_J = \pm^3/_2$ levels. A deeper understanding of the factors that mediate mixing of the M_J or M_S levels in mononuclear single-molecule magnets is thus needed, although influences, such as hyperfine coupling, deviations from purely axial molecular symmetry, and intermolecular dipolar interactions, could certainly contribute.[12,34] Notably, a combined theoretical and experimental study recently appeared,[35] wherein the Dy(III) ions of the species $[Dy_4K_2O(O\text{-}tBu)_{12}]\cdot C_6H_{14}$ were demonstrated to relax via an Orbach process at low temperature with U_{eff} values that closely followed the calculated energy gap between the ground and second-lowest-lying M_J level.

CONCLUSIONS AND OUTLOOK

Slow magnetic relaxation in mononuclear single molecule magnets is typically assessed via ac magnetic susceptibility, which limits the scope of the information that can be obtained due to current instrumental limitations. For instance, strict magnetostructural correlations between the coordination environment of the paramagnetic ion and U_{eff} can be hampered by an incorrect assessment of the relaxation process that is facilitating the magnetic relaxation. Here, we have employed Mössbauer spectroscopy to derive information about the magnetization dynamics of **1** and **2** that was unobtainable via conventional SQUID magnetometry, including the elucidation of the relaxation mechanism for **1** at high temperature and **2** at zero applied dc field. To further emphasize the potential utility of Mössbauer spectroscopy for accurate evaluation of U_{eff} values for mononuclear species, we note that an example of a mononuclear species displaying what is likely a Raman relaxation process over the temperature and ac frequency ranges possible with a conventional SQUID was recently reported.[6m] Though this observation was for a species with easy-plane anisotropy, a similar set of circumstances could have easily arisen in a system with a negative axial anisotropy, given the prevalence of curved Arrhenius plots (as evidenced in present and previous reports[4,6a,b,h,j]). Note that a full, comprehensive analysis of the relaxation behavior, enabled by a large investigated temperature range, would likely reveal U_{eff} in the presence of such complicated relaxation dynamics. In these particular cases, Mössbauer analysis, on account of the iron nuclei, would be facile. For mononuclear single molecule magnets based on other nuclei, however, other experimental means of detecting magnetic relaxation times at high frequency are clearly needed.

Among the reported mono- and multinuclear lanthanide clusters that exhibit slowly relaxing magnetic moments, a large fraction contains dysprosium(III). Dysprosium-161 is a Mössbauer active nuclide, with a sufficient abundance of 19% and easily detected γ-transition of 25 keV, but, unfortunately, its parent, the terbium-161 nuclide, has only a six-day half-life. The accessible relaxation time-domain[36,37] with dysprosium-161 is between about 0.01 and 2 ns. Hence, dysprosium-161 Mössbauer spectroscopy may become an informative technique to study the magnetic dynamics of dysprosium containing single-molecule magnets, albeit at laboratories that can easily prepare the source.

ASSOCIATED CONTENT

Supporting Information

Additional discussion of the quadrupole splittings, tables of temperature-dependent fitted Mössbauer parameters of **1** and **2**, and additional relaxation time plots. This material is available free of charge via the Internet at http://pubs.acs.org.

AUTHOR INFORMATION

Corresponding Authors

*E-mail: joe.zadrozny@gmail.com (J.Z.).
*E-mail: jrlong@berkeley.edu (J.R.L.).
*E-mail: Mihail.Atanasov@cec.mpg.de (M.A.).
*E-mail: frank.neese@cec.mpg.de (F.N.).
*E-mail: fgrandjean@ulg.ac.be (F.G.).
*E-mail: glong@mst.edu (G.J.L.).

Notes

The authors declare no competing financial interest.

ACKNOWLEDGMENTS

We thank Professor Christopher J. Chang at UC-Berkeley for the use of the Mössbauer spectrometer and Dr. Raphaël P. Hermann at Jülich Center for Neutron Science for his help for implementing the code for the Mössbauer spectral relaxation fits.

REFERENCES

(1) (a) Gorter, C. J. *Phys. Z.* **1938**, *39*, 815. (b) de Haas, W. J.; du Pré, F. K. *Physica* **1938**, *5*, 501. (b1) de Haas, W. J.; du Pré, F. K. *Physica* **1939**, *6*, 705. (c) Teunissen, P.; Gorter, C. J. *Physica* **1940**, *7*, 33. (d) Casimir, H. B. G.; Bijil, D.; du Pré, F. K. *Physica* **1941**, *8*, 449. (e) Gorter, C. J. *Paramagnetic Relaxation*; Elsevier Pub. Co.: New York, 1947.

(2) Gatteschi, D.; Sessoli, R.; Villain, J. *Molecular Nanomagnets*; Oxford University Press: New York, 2006.

(3) (a) Ishikawa, N.; Sugita, M.; Ishikawa, T.; Koshihara, S.-Y.; Kaizu, Y. *J. Am. Chem. Soc.* **2003**, *125*, 8694. (b) Ishikawa, N.; Sugita, M.; Ishikawa, T.; Koshihara, S.; Kaizu, S. *J. Phys. Chem. B* **2004**, *108*, 11265. (c) Ishikawa, N.; Sugita, M.; Wernsdorfer, W. *J. Am. Chem. Soc.* **2005**, *127*, 3650.

(4) (a) Freedman, D. E.; Harman, W. H.; Harris, T. D.; Long, G. J.; Chang, C. J.; Long, J. R. *J. Am. Chem. Soc.* **2010**, *132*, 1224. (b) Harman, W. H.; Harris, T. D.; Freedman, D. E.; Fong, H.; Chang, A.; Rinehart, J. D.; Ozarowski, A.; Sougrati, M. T.; Grandjean, F.; Long, G. J.; Long, J. R.; Chang, C. J. *J. Am. Chem. Soc.* **2010**, *132*, 18115.

(5) (a) Sorace, L.; Benelli, C.; Gatteschi, D. *Chem. Soc. Rev.* **2011**, *40*, 3092. (b) Rinehart, J. D.; Long, J. R. *Chem. Sci.* **2011**, *2*, 2078. (c) Woodruff, D. N.; Winpenny, R. E. P.; Layfield, R. A. *Chem. Rev.* **2013**, *113*, 5110.

(6) (a) Weismann, D.; Sun, Y.; Lan, Y.; Wolmerhauser, G.; Powell, A. K.; Sitzmann, H. *Chem.—Eur. J.* **2011**, *17*, 4700. (b) Lin, P.-H.; Smythe, N. C.; Gorelsky, S. L.; Maguire, S.; Henson, N. J.; Korobkov, I.; Scott, B. L.; Gordon, J. C.; Baker, R. T.; Murugesu, M. *J. Am. Chem. Soc.* **2011**, *133*, 15806. (c) Jurca, T.; Farghal, A.; Lin, P.-H.; Korobkov, I.; Murugesu, M.; Richeson, D. S. *J. Am. Chem. Soc.* **2011**, *133*, 15814. (d) Zadrozny, J. M.; Liu, J.; Piro, N. A.; Chang, C. J.; Hill, S.; Long, J. R. *Chem. Commun.* **2012**, *48*, 3927. (e) Zadrozny, J. M.; Long, J. R. *J. Am. Chem. Soc.* **2011**, *133*, 20732. (f) Vallejo, J.; Castro, I.; Ruiz-García, R.; Cano, J.; Julve, M.; Lloret, F.; De Munno, G.; Wernsdorfer, W.; Pardo, E. *J. Am. Chem. Soc.* **2012**, *134*, 15704. (g) Mossin, S.; Tran, B. L.; Adikari, D.; Pink, M.; Heinemann, F. W.; Sutter, J.; Szilagyi, R. K.; Meyer, K.; Mindiola, D. J. *J. Am. Chem. Soc.* **2012**, *134*, 13651. (h) Zadrozny, J. M.; Atanasov, M.; Bryan, A. M.; Lin, C.-Y.; Rekken, B. D.; Power, P. P.; Neese, F.; Long, J. R. *Chem. Sci.* **2013**, *4*, 125. (i) Zhu, Y.-Y.; Cui, C.; Zhang, Y.-Q.; Jia, J.-H.; Guo, X.; Gao, C.; Qian, K.; Jiang, S.-D.; Wang, B.-W.; Wang, Z.-M.; Gao, S. *Chem. Sci.* **2013**, *4*, 1802. (j) Zadrozny, J. M.; Xiao, D. J.; Atanasov, M.; Long, G. J.; Grandjean, F.; Neese, F.; Long, J. R. *Nature Chem.* **2013**, *5*, 577. (k) Zadrozny, J. M.; Telser, J.; Long, J. R. *Polyhedron* **2013**, *64*, 209. (l) Ishikawa, R.; Miyamoto, R.; Nojiri, H.; Breedlove, B. K.; Yamashita,

M. *Inorg. Chem.* **2013**, *52*, 8300. (m) Colacio, E.; Ruiz, J.; Ruiz, E.; Cremades, E.; Krzystek, J.; Caretta, S.; Cano, J.; Guidi, T.; Wernsdorfer, W.; Brechin, E. K. *Angew. Chem., Int. Ed.* **2013**, *52*, 9130.
(7) Mannini, M.; Pineider, F.; Sainctavit, P.; Danieli, C.; Otero, E.; Sciancalepore, C.; Talarico, A. M.; Arrio, M.-A.; Cornia, A.; Gatteschi, D.; Sessoli, R. *Nat. Mater.* **2009**, *8*, 194.
(8) (a) Leuenberger, M. N.; Loss, D. *Nature* **2001**, *410*, 789. (b) Ardavan, A.; Rival, O.; Morton, J. J. L.; Blundell, S. J.; Tyryshkin, A. M.; Timco, G. E.; Winpenny, R. E. P. *Phys. Rev. Lett.* **2007**, *98*, 057201. (c) Stamp, P. C. E.; Gaita-Ariño, A. *J. Mater. Chem.* **2009**, *19*, 1718.
(9) (a) Cremades, E.; Ruiz, E. *Inorg. Chem.* **2011**, *50*, 4016. (b) Atanasov, M.; Ganyushin, D.; Pantazis, D. A.; Sivalingam, K.; Neese, F. *Inorg. Chem.* **2011**, *50*, 7460. (c) Maganas, D.; Sottini, S.; Kyritsis, P.; Groenen, E. J. J.; Neese, F. *Inorg. Chem.* **2011**, *50*, 8741. (d) Baldovi, J. J.; Cardona-Serra, S.; Clemente-Juan, J. M.; Coronado, E.; Gaita-Ariño, A.; Palii, A. *Inorg. Chem.* **2012**, *51*, 12565. (e) Baldovi, J. J.; Cardona-Serra, S.; Clemente-Juan, J. M.; Coronado, E.; Gaita-Ariño, A. *Chem. Sci.* **2013**, *4*, 938. (f) Gomez-Coca, S.; Cremades, E.; Aliaga-Alcalde, N.; Ruiz, E. *J. Am. Chem. Soc.* **2013**, *135*, 7010.
(10) Atanasov, M. A.; Zadrozny, J. M.; Long, J. R.; Neese, F. *Chem. Sci.* **2013**, *4*, 139.
(11) (a) Orbach, R. *Proc. R. Soc. London, Ser. A* **1961**, *264*, 458. (b) Orbach, R. *Proc. R. Soc. London, Ser. A* **1961**, *264*, 485.
(12) Gatteschi, D.; Sessoli, R. *Angew. Chem., Int. Ed.* **2003**, *42*, 268.
(13) Walker, M. B. *Can. J. Phys.* **1968**, *46*, 1347.
(14) Carlin, R. L. *Magnetochemistry*; Springer: Berlin, Germany, 1986.
(15) Dattagupta, S.; Blume, M. *Phys. Rev. B* **1974**, *10*, 4540.
(16) Stoian, S. A.; Yu, Y.; Smith, J. M.; Holland, P. L.; Bominaar, E. L.; Münck, E. *Inorg. Chem.* **2005**, *44*, 4915.
(17) Reiff, W. M.; LaPointe, A. M.; Witten, E. H. *J. Am. Chem. Soc.* **2004**, *126*, 10206.
(18) LaPointe, A. M. *Inorg. Chim. Acta* **2003**, *345*, 359.
(19) (a) Neese, F. *WIRES Comput. Mol. Sci.* **2012**, *2*, 73. (b) Neese, F. with contributions from Becker, U.; Ganyushin, G.; Hansen, A.; Izsak, R.; Liakos, D. G.; Kollmar, C.; Kossmann, S.; Pantazis, D. A.; Petrenko, T.; Reimann, C.; Riplinger, C.; Roemelt, M.; Sandhöfer, B.; Schapiro, I.; Sivalingam, K.; Wennmohs, F.; Wezisla, B. and contributions from our collaborators: Kállay, M.; Grimme, S.; Valeev, E. *ORCA, An ab initio, DFT, and semiempirical SCF-MO package*, Version 2.9.1; Mülheim a.d.R. [The binaries of ORCA are free of charge for academic users for a variety of platforms].
(20) (a) Becke, A. D. *Phys. Rev. A* **1988**, *38*, 3098. (b) Perdew, J. P. *Phys. Rev. B* **1986**, *33*, 8822.
(21) Schafer, A.; Huber, C.; Ahlrichs, R. *J. Chem. Phys.* **1994**, *100*, 5829.
(22) Romelt, M.; Ye, S.; Neese, F. *Inorg. Chem.* **2009**, *48*, 784.
(23) (a) Blume, M.; Tjon, J. A. *Phys. Rev.* **1968**, *165*, 446. (b) Tjon, J. A.; Blume, M. *Phys. Rev.* **1968**, *165*, 456.
(24) Mørup, S. In *The Time Domain in Surface and Structural Dynamics NATO-ASI Series C*; Long, G. J., Grandjean, F., Eds.; Kluwer: Dordrecht, The Netherlands, 1988; Vol. *228*.
(25) Wickman, H. H. In *Mössbauer Effect Methodology*; Gruvermann, I. J., Ed.; Plenum Press: New York, 1966.
(26) Shenoy, G. K.; Wagner, F. E.; Kalvius, G. M. In *Mössbauer Isomer Shifts*; Shenoy, G. K., Wagner, F. E., Eds.; North-Holland, Amsterdam, The Netherlands, 1978; p 49.
(27) Owen, T.; Grandjean, F.; Long, G. J.; Domasevitch, K. V.; Gerasimchuk, N. N. *Inorg. Chem.* **2008**, *47*, 8704.
(28) Hazra, S.; Sasmal, S.; Fleck, F.; Grandjean, F.; Sougrati, M. T.; Ghosh, M.; Harris, T. D.; Bonville, P.; Long, G. J.; Mohanta, S. *J. Chem. Phys.* **2011**, *134*, 174507.
(29) Novák, P.; Wagner, F. R. *Phys. Rev. B* **2002**, *66*, 184434.
(30) (a) Schünemann, V.; Paulsen, H. In *Applications of Physical Methods to Inorganic and Bioinorganic Chemistry*; Scott, R. A., Lukehart, C. M., Eds.; Wiley: New York, 2007; p 243. (b) Greenwood, N. N.; Gibb, T. C. In *Mössbauer Spectroscopy*; Chapman and Hall: London, U.K., 1971.
(31) Klatyk, J.; Schnelle, W.; Wagner, F. R.; Niewa, R.; Novák, P.; Kniep, R.; Waldeck, M.; Ksenofontov, V.; Gütlich, P. *Phys. Rev. Lett.* **2002**, *88*, 207202.
(32) Ingalls, R. *Phys. Rev.* **1964**, *133*, A787.
(33) (a) Sessoli, R.; Hui, L.; Schake, A. R.; Wang, S.; Vincent, J. B.; Folting, K.; Gatteschi, D.; Christou, G.; Hendrickson, D. N. *J. Am. Chem. Soc.* **1993**, *115*, 1804. (b) Sessoli, R.; Gatteschi, D.; Caneschi, A.; Novak, M. A. *Nature* **1993**, *365*, 141.
(34) Prokof'ev, N. V.; Stamp, P. C. E. *Rep. Prog. Phys.* **2000**, *63*, 669.
(35) Blagg, R. J.; Ungur, L.; Tuna, F.; Speak, J.; Comar, P.; Collison, D.; Wernsdorfer, W.; McInnes, E. J. L.; Chibotaru, L. F.; Winpenny, R. E. P. *Nat. Chem.* **2013**, *5*, 673−678.
(36) Hufner, S.; Wickman, H. H.; Wagner, C. E. *Phys. Rev.* **1968**, *169*, 247.
(37) Khurgin, B.; Nowik, I.; Rakavy, M.; Ofer, S. *J. Phys. Chem. Solids* **1970**, *31*, 49.